Supplementary Information

Supplementary Materials and Methods

Study design

The objective of this study was to determine the neural circuits involved in kidney protection induced by VNS. First, we performed optogenetic VNS in *Chat-ChR2*, *Vglut2-ChR2* and control mice before kidney IRI surgery, and we found that efferent fiber stimulation or sensory afferent fiber stimulation both confer kidney protection. Then we performed splenectomy and adoptive transfer experiments in *Chat-ChR2*, *Vglut2-ChR2* and control mice to show that splenocytes play a critical role. We further performed a series of experiments in *Vglut2-ChR2* and control mice to identify the downstream pathway of afferent fiber stimulation. Then we hypothesized that C1 neurons in the medulla oblongata mediate the protective effect of vagus afferent fiber stimulation against kidney IRI based on our previous work (1). To test this hypothesis, we bilaterally microinjected AAV2-DIO-taCasp3-TEVp into the RVLM of *Dbh-Cre* mice to selectively ablate C1 neurons without affecting other types of neurons and performed electrical (distal or central) VNS in these mice. We also used Sprague-Dawley rats to demonstrate that vagal afferent stimulation activates the sympathetic nervous system (splenic, renal and lumbar) because of the difficulty to record from these nerves (especially splenic nerve) in mice. Sample size was determined based on previous pilot and published experiments (1, 2). No data were excluded from the analysis. Experiments were performed using littermates, which facilitates appropriate randomization. Within the littermate groups, animals were selected for IRI or sham surgeries at random. IRI surgeries were performed by an operator blinded to experimental setting including genotype. Plasma creatinine measurements and histological analysis were performed by investigators blinded to experimental setting. Plasma corticosterone and tissue norepinephrine levels were measured by an independent core facility in a blinded fashion.

Plasma creatinine/cytokine measurement, renal histology, and real-time PCR

Plasma was prepared by centrifuging heparinized blood at 7,000 g for 5 min. Plasma creatinine was determined by using an enzymatic method as per the manufacturer's protocol (Diazyme Laboratories) that we have validated using LC-MS (2). Plasma cytokine levels (TNFα and IL-6) were determined by ELISA as per the

manufacturer's protocol (Thermo Fisher Scientific). Plasma measurements were performed by investigators blinded to experimental setting. The extent of kidney injury was assessed using H&E-stained kidney sections (5 μm) as previously described (2). The sections were viewed by light microscopy (Zeiss AxioImager Z1 microscope, Carl Zeiss Microscopy). Photographs were taken with an AxioCam MRc camera (Zeiss), and brightness/contrast and white balance adjustments were made using StereoInvestigator software (Version 11; MBF Bioscience). The extent of kidney injury was assessed in an unbiased, systematic manner using design-based stereology to achieve statistically accurate random sampling of kidney sections, yielding the percentage of total area of the section occupied by injured tubules. The investigator was blinded to the experimental identity of the sections. Sections were imaged by using a Zeiss Axio Imager Z1 Microscope fitted with motorized focus drives and motorized XYZ microscope stage and integrated to a work station running StereoInvestigator software (MBF Bioscience). The area fraction fractionator probe was used for stereological analysis of the fractional area of the section occupied by tubular damage. The following parameters were defined: counting frame, 400 x 400 μm; sample grid, 800 x 800 μm; grid spacing, 85 μm. These values were determined empirically such that adequate numbers of sample sites were visited and adequate numbers of markers (indicating injured tubules) were acquired, in keeping with accepted counting rules for stereology. Injured tubules were identified based on the presence of cast formation, tubule dilation, and/or tubular epithelial denucleation. A total of 275 ± 7.3 (mean ± s.e.m.) grid sites was evaluated per section. For immunofluorescent labeling of kidney and spleen sections, samples were prepared and analyzed as previously described (3). Periodate-lysine-paraformaldehyde-fixed frozen sections were stained with an anti-Ly6G antibody (rat monoclonal, 1:2,500, MAB1037, R&D Systems) and anti-TH antibody (sheep polyclonal, 1:1,000; Millipore #AB1542; EMD Millipore) followed by Cy3-tagged anti-rat IgG (1:500, Jackson ImmunoResearch Laboratories) and Cy3-tagged anti-sheep IgG (1:500, Jackson ImmunoResearch Laboratories), respectively. Quantification of Ly6G positive area was done by averaging total Ly6G positive pixels of ten random outer medulla fields (at 200X) per kidney section with ImageJ software. Renal mRNA was isolated by following the ethanol-precipitation method, and RNA concentration was determined based on

spectrophotometric determination of a 260/280 ratio. cDNA was generated from the resultant tissue RNA using the iScript cDNA Synthesis Kit (Bio-Rad) as described by the manufacturer. Resultant cDNA was then used to determine relative mRNA expression of *Havcr1* (Kim-1) and *Actb* (b-actin) using the iTAC Universal SYBR Green Supermix (Bio-Rad). Primers used were as follows:

Havcr1 (forward): TGCTGCTACTGCTCCTTGTGAG,

(reverse): GGCAACCACGCTTAGAGATGC;

Actb (forward): AAGATCAAGATCATTGCTCCTCCTG,

(reverse): AAACGCAGCTCAGTAACAGTCC;

Tnf (forward): CCTCCCTCTCATCAGTTCTATGG,

(reverse): CGTGGGCTACAGGCTTGTC;

Il6 (forward): TGGCTAAGGACCAAGACCATCCAA,

(reverse): AACGCACTAGGTTTGCCGAGTAGA;

Il1b (forward): AATGACCTGTTCTTTGAAGTTGAC,

(reverse): GTGATACTGCCTGCCTGAAG;

Cxcl1 (forward): TGGCTGGGATTCACCTCAAGAACA,

(reverse): TGTGGCTATGACTTCGGTTTGGGT;

Cxcl2 (forward): AAAGTTTGCCTTGACCCTGAAGCC,

(reverse): TTTCCAGGTCAGTTAGCCTTGCCT.

Rat experiments (VNS, sympathetic nerve activity recording, IRI)

For sympathetic nerve activity recording, Sprague-Dawley rats were anesthetized with a mixture of urethane (500 mg/kg) and α-chloralose (50 mg/kg) given i.p. Depth of anesthesia was assessed by absence of the corneal and hindpaw withdrawal reflexes. Additional anesthetic was administered as necessary (10% of the original dose, i.p.). Body temperature was maintained at 37.0 ± 0.5 °C with a servo-controlled temperature pad (TC-1000; CWE) and a blanket. All surgical procedures were performed under aseptic conditions. Mechanical

ventilation with 100% oxygen was maintained through a tracheal tube. To record the splenic/lumber and renal sympathetic nerve activity during VNS, the postganglionic sympathetic nerve was isolated through a laparotomy and a right flank incision, respectively. Two stainless-steel electrodes (AS633; Cooner Wire) were placed around the postganglionic sympathetic nerve. The nerve and electrodes were covered and fixed with silicone gel (Kwik-Sil; World Precision Instruments). To perform central VNS, the left cervical vagus nerve was isolated via a midline cervical incision and transected, and then two stainless-steel electrodes (AS633; Cooner Wire) were placed at the central end of the transected vagus nerve. The electrical stimulation (square wave; 1, 3, and 5 Hz; 150 μA intensity; 1-ms pulses) was applied using a Grass model S88 stimulator and stimulus isolation unit (Astro-Med Inc.). For sham VNS, rats underwent similar procedures but the electrodes and stimulator were disconnected. All analog data were acquired on a computer via a Micro3 1401 digitizer (CED) and processed using Spike 2 software (v7.06; CED). The sympathetic nerve activities were band-pass filtered (100–1000 Hz), rectified and integrated.

To confirm that VNS with the parameters used for nerve recordings is protective against kidney IRI in rats, another group of rats was anesthetized with an i.p. injection of ketamine (120 mg/kg) and xylazine (12 mg/kg). The electrical stimulation (square wave, 5 Hz, 150 μA intensity, 1-ms pulses) at left cervical vagus nerve was applied for 10 min as described above. Twenty-four hours after VNS, rats were anesthetized with an i.p. injection of ketamine (120 mg/kg) and xylazine (12 mg/kg). Bilateral kidney IRI was performed through flank incisions by clamping the renal pedicles for 45 min. The clamps were then removed and the wound sutured after restoration of blood flow was visually observed. Rats received buprenorphine-SR (1.0 mg/kg) as a postoperative analgesic. Twenty-four hours after IRI, rats were euthanized for measurement of plasma creatinine.

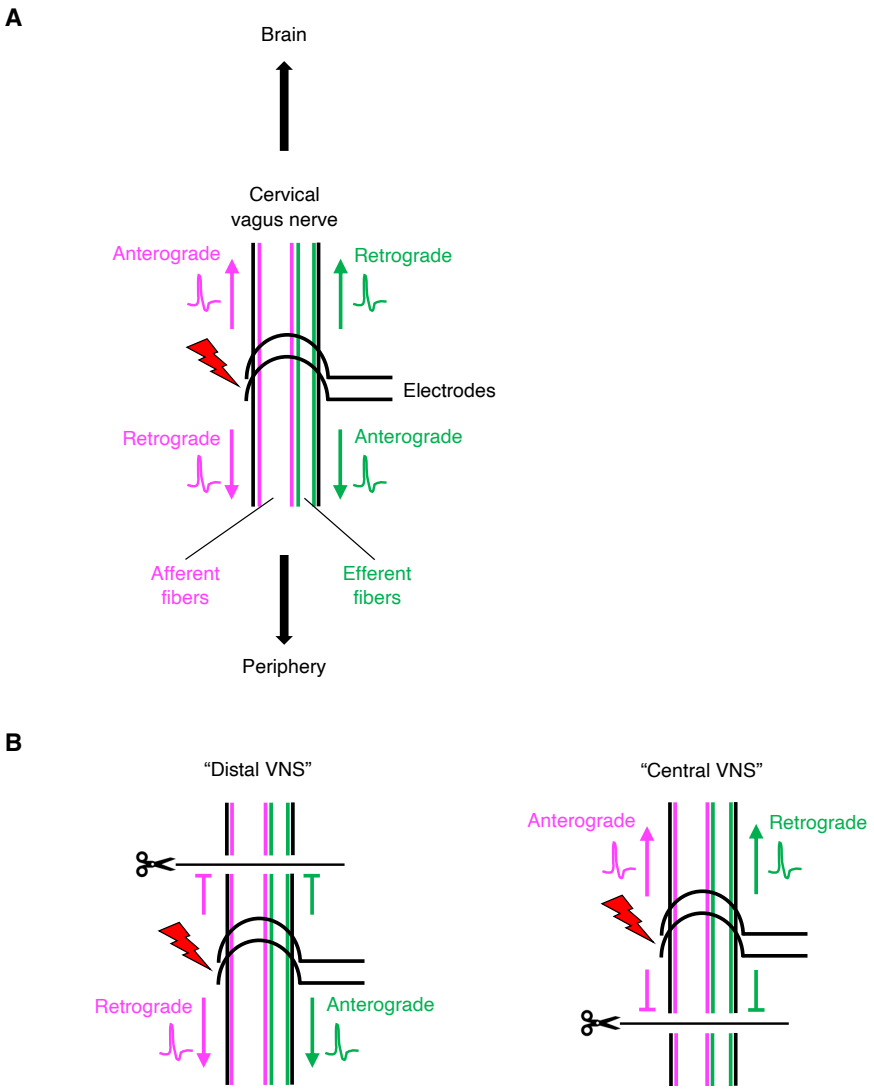

Supplementary Fig. 1. Four distinct pathways in the cervical vagus nerve activated by electrical stimulation. (**A**) Illustration depicting four distinct pathways in the cervical vagus nerve activated by electrical vagus nerve stimulation (VNS). Vagus nerve contains motor (efferent) and sensory (afferent) fibers. Action potentials elicited by VNS are transmitted in two directions (anterograde and retrograde) in each type of fibers. (**B**) Illustration depicting two distinct pathways in the cervical vagus nerve activated by "distal VNS" and "central VNS". The terms distal and central VNS are used to describe the direction of impulse flow resulting from electrical stimulation at the distal (towards the periphery) and central end (towards the brain) of the transected vagus nerve, respectively. Local anesthesia can also be used to block nerve conduction. Note that these experimental paradigms are still not selective for a single pathway but are a combination of two distinct pathways in efferent and afferent fibers.

Validation of mouse models for selective vagus efferent versus vagus afferent fiber stimulation (Supplementary Fig. 2-6)

Chat-ChR2 (for selective optogenetic efferent fiber stimulation) and *Vglut2-ChR2* (for selective optogenetic afferent fiber stimulation) mice were created and validated (Supplementary Fig. 2). Expression of ChR2-eYFP was confirmed by directly observing eYFP fluorescence in the cervical vagus nerve trunk (Supplementary Fig. 3, A-C). We confirmed that ChR2 is selectively expressed in vagal efferents in *Chat-ChR2* mice, and in vagal afferents in *Vglut2-ChR2* mice (Supplementary Fig. 3, D-N). In *Chat-ChR2* mice (Supplementary Fig. 3, D-H), ChR2-eYFP was expressed in cholinergic neurons (ChAT+) in the dorsal motor nucleus of the vagus (DMV) and the nucleus ambiguus (nAmb) (Supplementary Fig. 3, D-F), but not in the nodose ganglion (Supplementary Fig. 3, G and H). ChR2-eYFP was expressed in cholinergic axons of DMV neurons (highlighted by arrows in Supplementary Fig. 3, E and F). In *Vglut2-ChR2* mice, ChR2-eYFP was absent from neurons in the DMV and nAmb (Supplementary Fig. 3, I-K), and present in neuronal cell bodies in the nodose ganglion (Supplementary Fig. 3, L and M). ChR2-eYFP axons were observed in the vagal afferents in the solitary tract (highlighted by arrows in Supplementary Fig. 3, J and K). No ChR2-eYFP was observed in Cre-negative control mice (Supplementary Fig. 3N). Blue laser application to the cervical vagus nerve evoked action potentials in the vagus nerve thereby confirming functional expression of ChR2 in *Chat-ChR2* (Supplementary Fig. 4A) and *Vglut2-ChR2* (Supplementary Fig. 4B) mice, whereas the laser light did not evoke action potentials in Cre-negative control mice (Supplementary Fig. 4C). We also confirmed the selectivity of stimulation (efferent vs. afferent fibers) in *Chat-ChR2* and *Vglut2-ChR2* mice by observing changes in heart rate and respiratory rate during optogenetic VNS. Selective stimulation of vagus efferent fibers decreases heart rate without changing respiratory rate, since these fibers innervate the sinoatrial and atrioventricular nodes (4). Optogenetic VNS in *Chat-ChR2* mice resulted in a significant decrease in heart rate as expected (Supplementary Fig. 5A). In contrast, selective stimulation of vagus afferent fibers decreases respiratory rate, which is known as the Hering-Breuer inflation reflex (5). Optogenetic VNS in *Vglut2-ChR2* mice resulted in a significant decrease in both heart rate and respiratory rate (Supplementary Fig. 5B); the

former change is probably through a vago-vagal reflex, in which stimulation of vagus afferent fibers leads to activation in the dorsal motor nucleus of vagus efferent neurons. The laser light had no effect on heart rate or breathing in Cre-negative control mice (Supplementary Fig. 5, C and D). Next we transected the cervical vagus nerve and applied blue laser light to the central or distal end of the transected vagus nerve (Supplementary Fig. 5, E and F). In *Chat-ChR2* mice, stimulation of the distal end decreased heart rate but stimulation of the central end did not change heart rate or respiratory rate (Supplementary Fig. 5E). In *Vglut2-ChR2* mice, stimulation of the central end decreased both heart rate and respiratory rate whereas stimulation of the distal end had no effect (Supplementary Fig. 5F). Unchanged heart rate during stimulation at the distal end of the cut vagus in *Vglut2-ChR2* mice excluded the possibility that vagal efferent fibers were stimulated in *Vglut2-ChR2* mice. We also applied bupivacaine, a local anesthetic, directly to the cervical vagus nerve to block nerve conduction and then applied blue laser to the central or distal side of the anesthetized area, which yielded the same results as those in the experiments with transected vagus nerve (Supplementary Fig. 6, A and B). The efficacy of bupivacaine application in nerve conduction blockade was confirmed by the observation that light-evoked retrograde action potentials were blocked by bupivacaine applied between the stimulation site and recording site (Supplementary Fig. 6C). In addition, 90 min after blue laser application to the left cervical vagus nerve for 10 min (5 Hz), a significantly greater number of c-Fos positive NTS neurons was observed in *Vglut2-ChR2* mice than in *Chat-ChR2* and control mice (Supplementary Fig. 6D). These results suggest that efferent and afferent fibers are selectively stimulated by optogenetic VNS in *Chat-ChR2* and *Vglut2-ChR2* mice, respectively. Stimulation at different frequencies revealed the frequency response of changes in heart rate and respiratory rate in these mice (Supplementary Fig. 5, C and D). 5 Hz was used in the remainder of the optogenetic VNS experiments (mostly to investigate its protective effect against kidney injury) since stimulation at 5 Hz produced a small (< 10%) but reliable reduction in heart rate and respiratory rate.

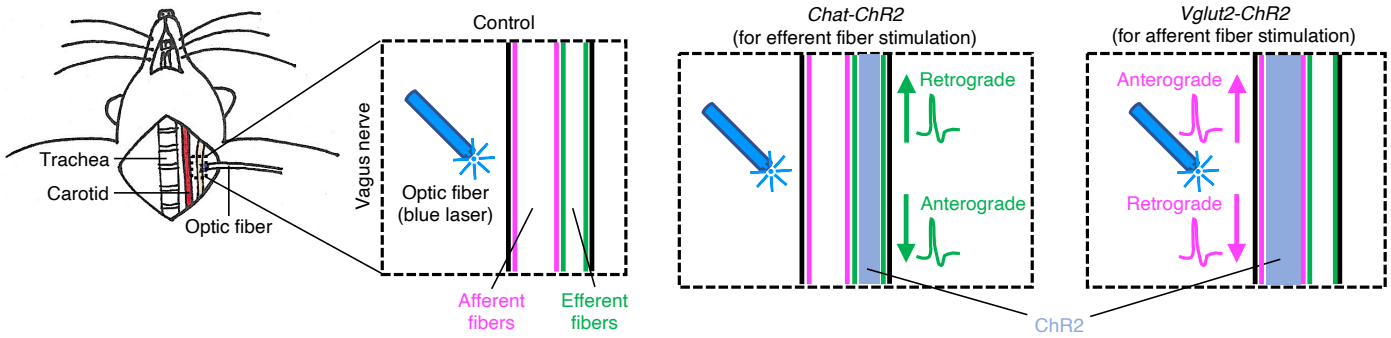

Supplementary Fig. 2. Illustration depicting the strategy for optogenetic vagus nerve stimulation in *Chat-ChR2* (for selective efferent fiber stimulation) and *Vglut2-ChR2* (for selective afferent fiber stimulation) mice. The left cervical vagus nerve was surgically exposed in anesthetized mice and blue laser was used for stimulation. ChR2 expression in the vagus nerve was limited to efferent and afferent fibers (blue shading) in *Chat-ChR2* and *Vglut2-ChR2* mice, respectively. Action potentials elicited by optogenetic stimulation are transmitted in two directions (anterograde and retrograde) in ChR2-expressing fibers.

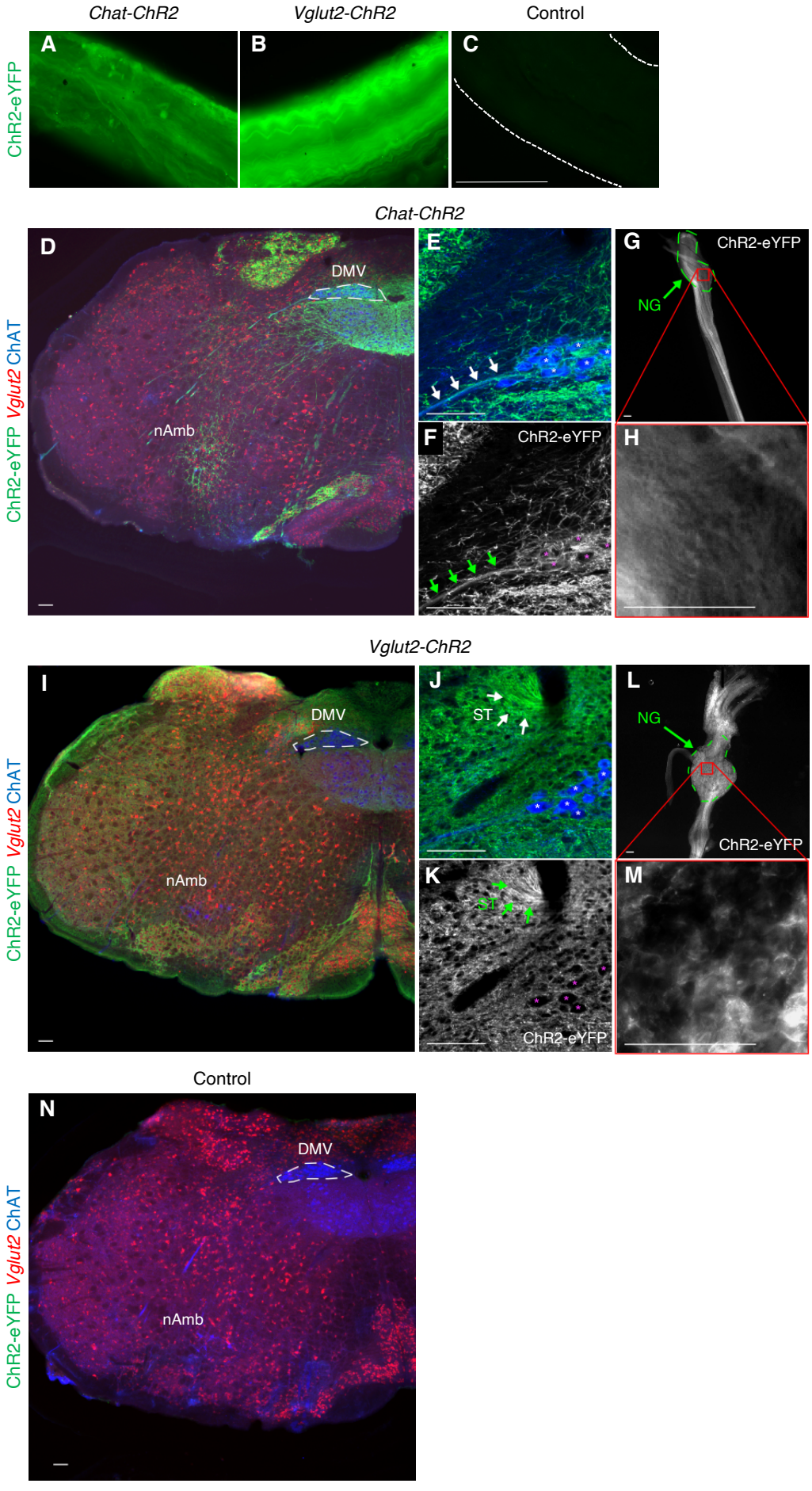
Chat-ChR2
Vglut2-ChR2
Control
A
B
C
ChR2-eYFP
Chat-ChR2
D
DMV
nAmb
E
F
ChR2-eYFP
G
ChR2-eYFP
NG
H
ChR2-eYFP Vglut2 ChAT
Vglut2-ChR2
I
DMV
nAmb
J
ST
K
ST
ChR2-eYFP
L
NG
ChR2-eYFP
M
ChR2-eYFP Vglut2 ChAT
Control
N
DMV
nAmb
ChR2-eYFP Vglut2 ChAT

Supplementary Fig. 3. ChR2 is selectively expressed in vagal efferents in *Chat-ChR2* mice, and in vagal afferents in *Vglut2-ChR2* mice. (**A-C**) Fluorescence microscopy images of the left cervical vagus nerve trunk from *Chat-ChR2* (**A**), *Vglut2-ChR2* (**B**), and control (**C**) mice. eYFP is fused with ChR2 in these mice. Note that the signal intensities are consistent with the fact that the vagus is composed of about 80% sensory afferent fibers and about 20% motor efferent fibers (6), which is nominally reflected in the illustrations depicting afferent and efferent fibers in the relevant figures. (**D-F**) Representative images of ChR2-eYFP (green), *Vglut2* (red), and ChAT (blue) in the brainstem of *Chat-ChR2* mice. Note that ChR2-eYFP was expressed in the dorsal motor nucleus of the vagus (DMV), the nucleus ambiguus (nAmb) (**D**), and the axons (highlighted by arrows) originating from ChAT-positive cell bodies (asterisks) in DMV (**E** and **F**). (**G** and **H**) Cervical vagus nerve and nodose ganglion (NG) in *Chat-ChR2* mice. Fibers but no cell bodies were positive for ChR2-eYFP (white). These findings indicate selective expression of ChR2 in vagal efferents in *Chat-ChR2* mice. (**I-K**) Representative images of ChR2-eYFP (green), *Vglut2* (red), and ChAT (blue) in the brainstem of *Vglut2-ChR2* mice. Note that ChAT-expressing neurons (e.g., DMV, nAmb) did not express ChR2-eYFP (asterisks: ChAT-positive cell bodies in DMV), whereas ChR2-eYFP-positive fibers were observed in the solitary tract (ST, highlighted by arrows). (**L** and **M**) Cervical vagus nerve and NG in *Vglut2-ChR2* mice. Fibers and cell bodies were positive for ChR2-eYFP (white). These findings indicate selective expression of ChR2 in vagal afferents in *Vglut2-ChR2* mice. (**N**) Representative images of ChR2-eYFP (green), *Vglut2* (red), and ChAT (blue) in the brainstem of Cre-negative control mice. No expression of ChR2-eYFP was observed. Bregma level for brainstem sections: -7.47 mm, scale bar: 200 μm in all figures. On the brainstem sections, ChR2-eYFP and ChAT protein were detected by immunostaining, and *Vglut2* mRNA was detected by in situ hybridization. Expression of ChR2-eYFP in the cervical vagus nerve and NG was detected by directly observing eYFP fluorescence.

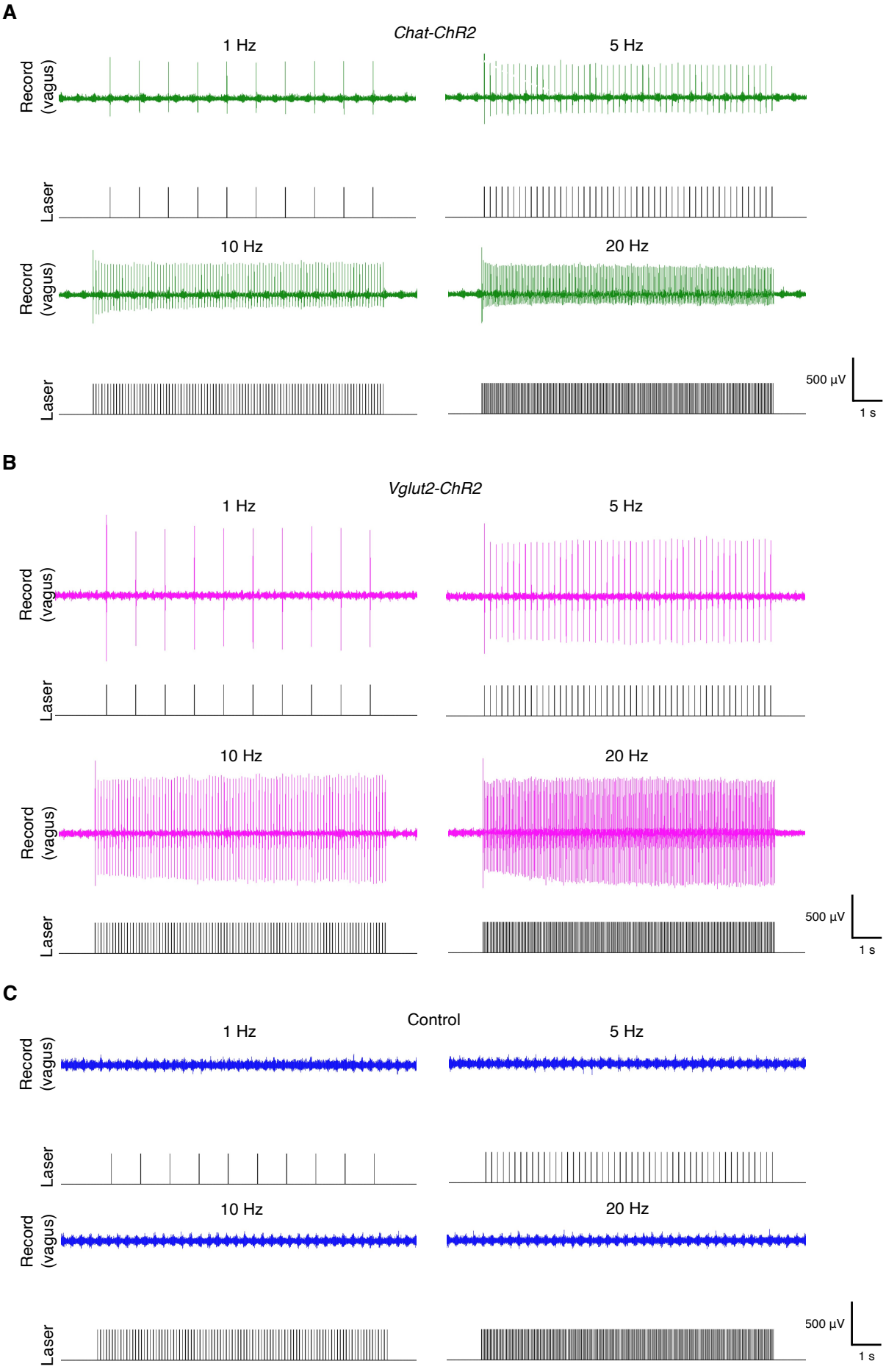
A
Chat-ChR2
1 Hz
5 Hz
Record (vagus)
Laser
10 Hz
20 Hz
500 µV
1 s
B
Vglut2-ChR2
1 Hz
5 Hz
Record (vagus)
Laser
10 Hz
20 Hz
500 µV
1 s
C
Control
1 Hz
5 Hz
Record (vagus)
Laser
10 Hz
20 Hz
500 µV
1 s

Supplementary Fig. 4. Function of ChR2 in the cervical vagus nerve of *Chat-ChR2* and *Vglut2-ChR2* mice. Whole nerve electrophysiological recordings at left cervical vagus nerve in *Chat-ChR2* (**A**), *Vglut2-ChR2* (**B**), and control mice without ChR2 expression (**C**). The left cervical vagus nerve was surgically exposed in anesthetized mice and illuminated by blue laser (1, 5, 10, 20 Hz) to activate ChR2-expressing fibers. Note that each blue laser application successfully evoked an action potential in *Chat-ChR2* (**A**) and *Vglut2-ChR2* (**B**) mice whereas no action potential was evoked in control mice (**C**).

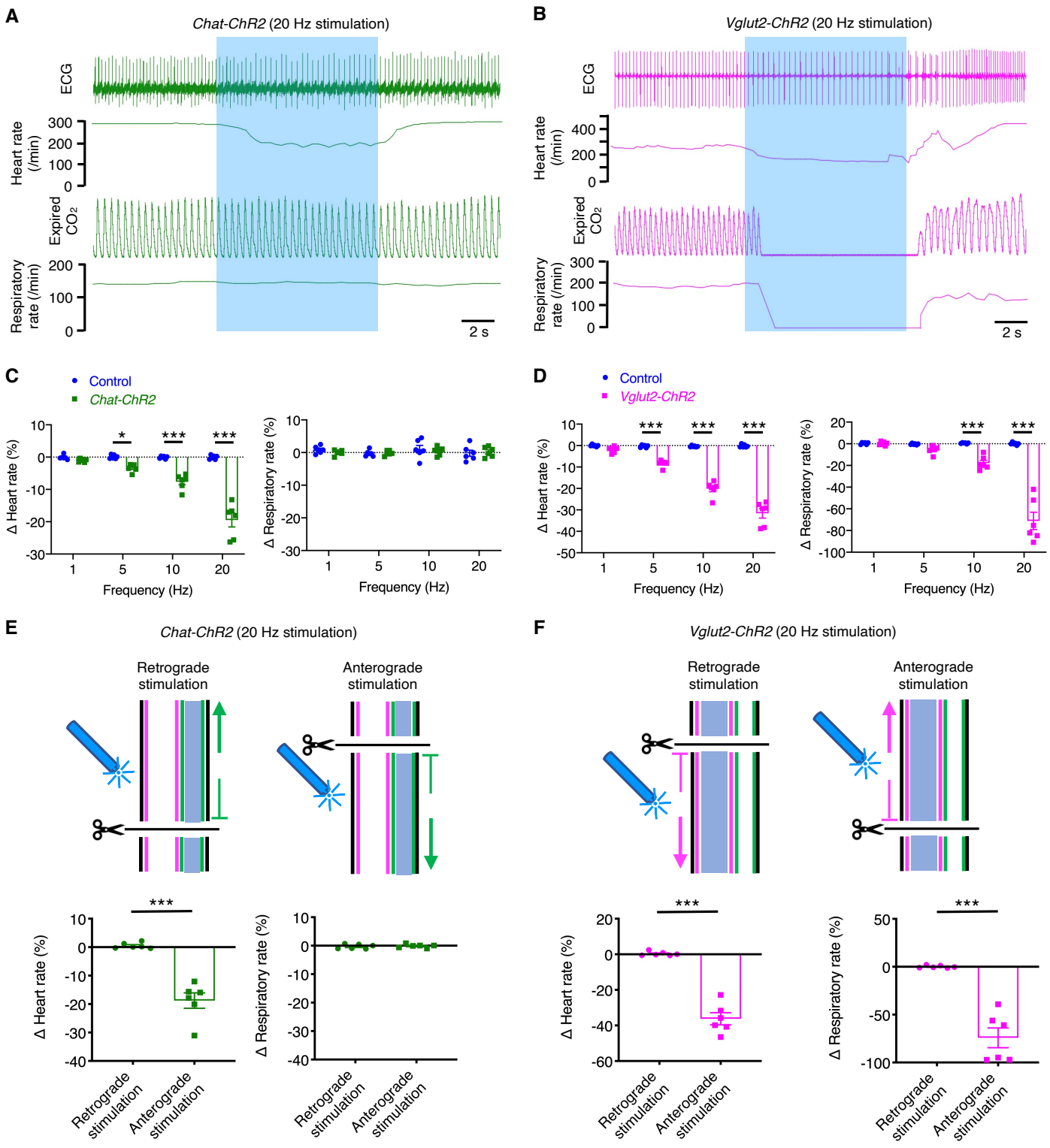

Supplementary Fig. 5. Proof of selective stimulation in *Chat-ChR2* and *Vglut2-ChR2* mice. (**A** and **B**) Representative measurements of heart rhythm (ECG) and respiratory rhythm (expired CO_2) following optogenetic vagus nerve stimulation (blue shading; 20 Hz, 10 s) in *Chat-ChR2* (**A**) and *Vglut2-ChR2* (**B**) mice. (**C** and **D**) Frequency response data summarizing the effects of optogenetic vagus nerve stimulation (10 s) on

heart rate and respiratory rate in *Chat-ChR2* (**C**), *Vglut2-ChR2* (**D**), and control (**C** and **D**) mice. (**E** and **F**) Changes in heart rate and respiratory rate following optogenetic retrograde versus anterograde vagus nerve stimulation (20 Hz, 10 s) in *Chat-ChR2* (**E**) and *Vglut2-ChR2* (**F**) mice. The left cervical vagus nerve was transected and blue laser was applied to the central or distal end for retrograde or anterograde stimulation. n = 6 in each group (**C**-**F**). Data are represented as mean ± s.e.m. *$P < 0.05$ and ***$P < 0.001$ by two-way ANOVA with post hoc Sidak test (**C** and **D**) or unpaired two-sided Student's *t* test (**E** and **F**).

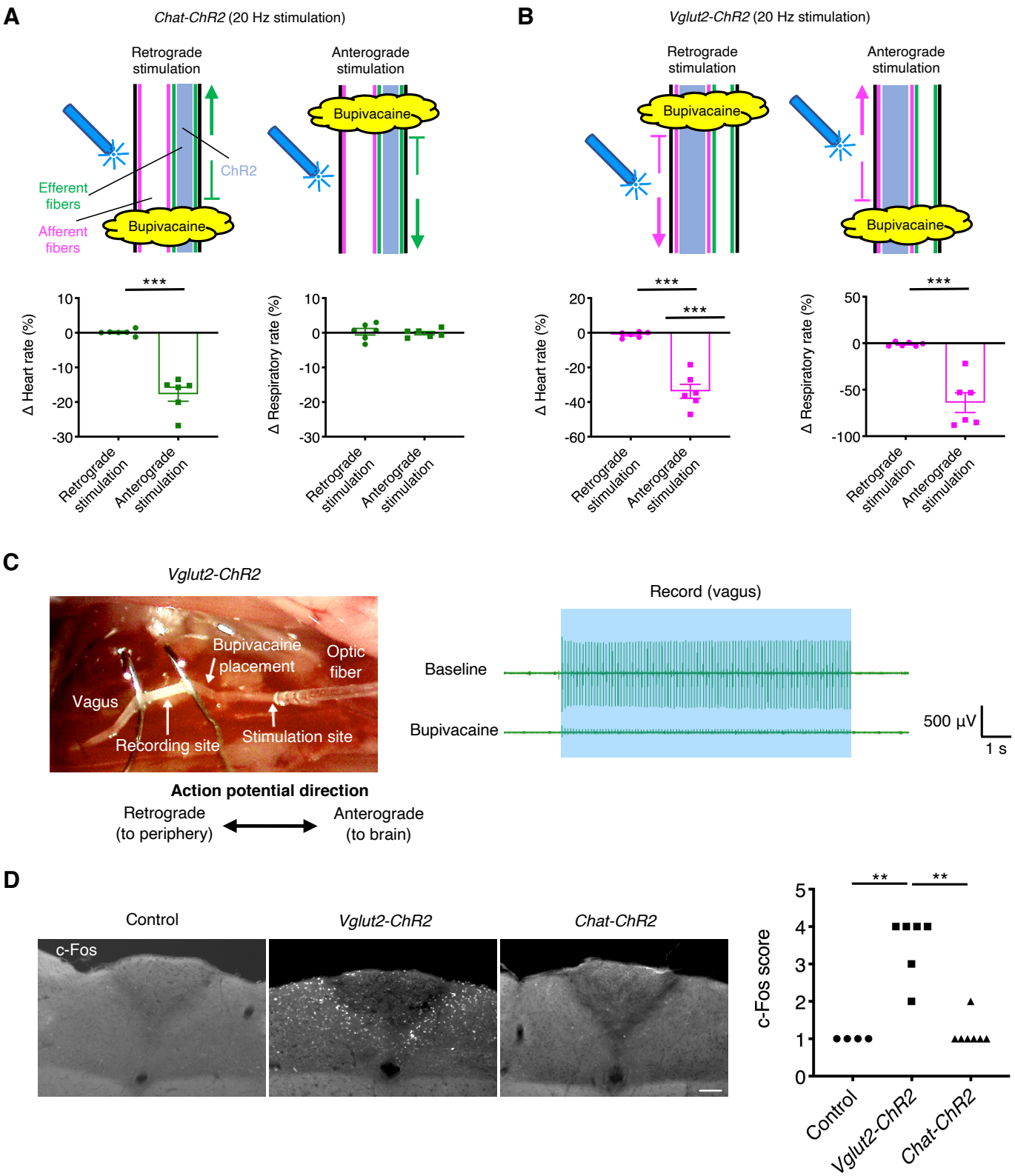

Supplementary Fig. 6. Proof of selective stimulation and effect of bupivacaine application to the vagus nerve in blocking nerve conduction. (**A** and **B**) Changes in heart rate and respiratory rate following optogenetic retrograde versus anterograde vagus nerve stimulation (20 Hz, 10 s) in *Chat-ChR2* (**A**) and *Vglut2-*

ChR2 (**B**) mice. Bupivacaine was directly applied to the left cervical vagus nerve to block nerve conduction, and blue laser was applied to the central or distal side of the anesthetized area for selective retrograde or anterograde stimulation of efferent (*Chat-ChR2* mice) or afferent fibers (*Vglut2-ChR2* mice). Blue shading represents fibers that express ChR2 and that can be activated by blue laser. n = 6 in each group. Data are represented as mean ± s.e.m. ***$P < 0.001$ by unpaired two-sided Student's *t* test. (**C**) Effect of bupivacaine application to the vagus nerve on evoked action potentials in *Vglut2-ChR2* mice with the experimental set-up. The cervical vagus nerve was surgically exposed in anesthetized mice and illuminated by blue laser (blue shading, 10 Hz) with or without bupivacaine application while action potentials were recorded at a distal site. Note that light stimulation at baseline produced large compound action potentials in the retrograde direction and these action potentials were blocked by bupivacaine applied between the stimulation site and recording site. This experiment was repeated in *Chat-ChR2* mice. (**D**) c-Fos immunoreactivity in the nucleus tractus solitarius (NTS; coronal plane, -7.48 mm from bregma) after selective stimulation. Cre-negative control (n = 4), *Vglut2-ChR2* (for afferent fiber stimulation, n = 6), and *Chat-ChR2* (for efferent fiber stimulation, n = 7) mice were euthanized 90 min after blue laser application to the left cervical vagus nerve (5 Hz, 10 min). Sections were scored blind for c-Fos expression on a scale of 1-4 with 1 for little to no expression and 4 for greatest expression. **$P < 0.01$ by Kruskal-Wallis with Dunn's test. Scale bar: 100 μm.

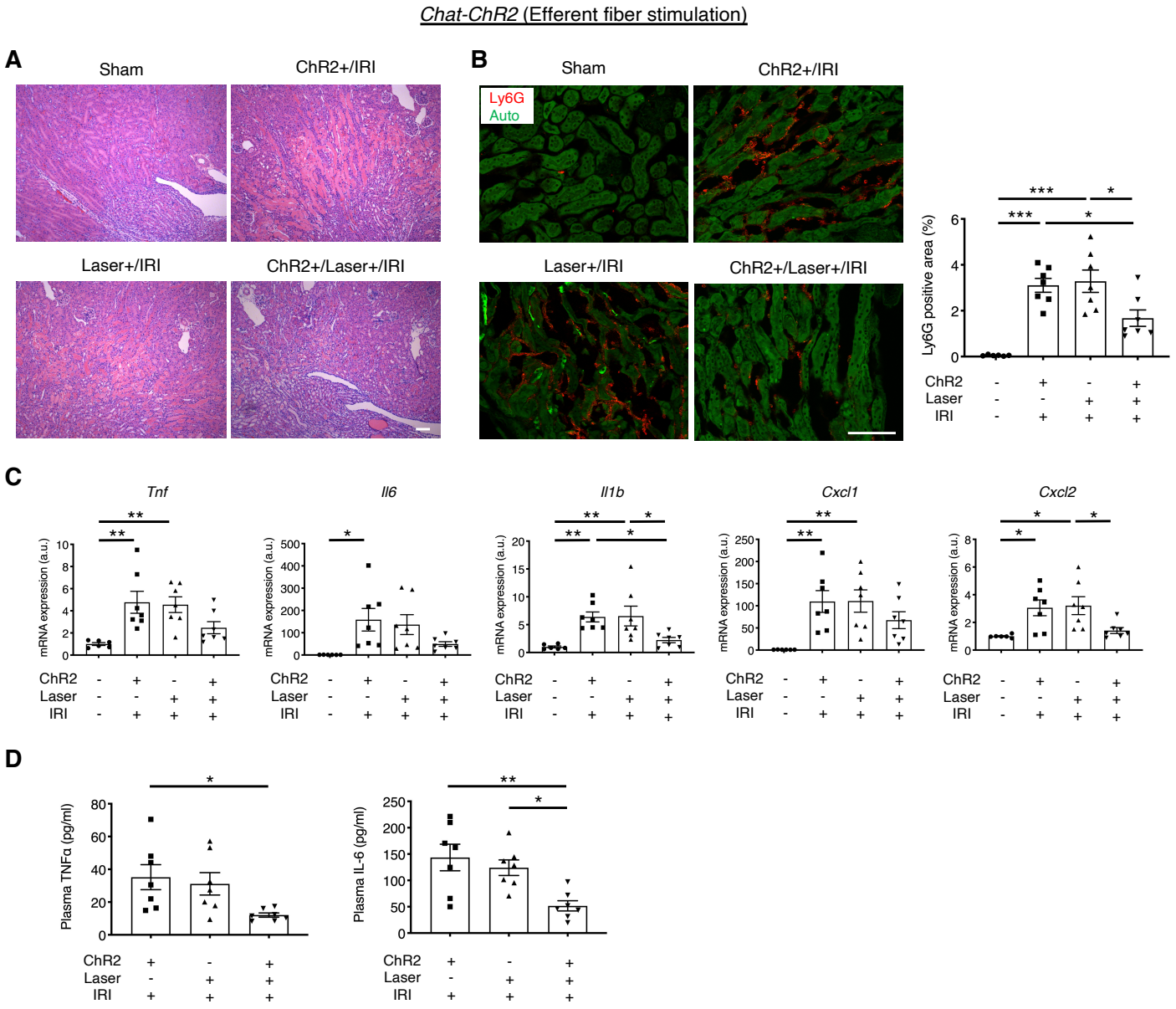

Supplementary Fig. 7. Optogenetic stimulation of vagus efferent fibers protects kidneys against IRI (related to Fig. 1). (**A-D**) Effect of selective efferent fiber stimulation (5 Hz, 10 min) on kidney injury (**A-C**) and plasma cytokine levels (**D**) at 24 h after sham or bilateral kidney IRI in *Chat-ChR2* and control mice. (**A**) Photomicrographs taken at lower magnification of H&E staining of representative kidney sections (higher magnification and quantitative analysis of acute tubular necrosis in Fig. 1D). (**B**) Neutrophil staining (Ly6G, red) of kidney with quantification of Ly6G positive area as a percentage of the total surface area of kidney section. Auto: autofluorescence (green). (**C**) Transcript levels of inflammatory cytokines/chemokines (*Tnf*, *Il6*, *Il1b*, *Cxcl1*, *Cxcl2*) in the kidneys. (**D**) Plasma TNFα and IL-6 at 24 h after bilateral kidney IRI were determined by ELISA. Plasma TNFα and IL-6 were under detection threshold in sham IRI group. n = 6 in sham IRI group

and n = 7 in IRI groups (**B**-**D**). Scale bars, 100 μm. Data are represented as mean ± s.e.m. *$P < 0.05$, **$P < 0.01$, and ***$P < 0.001$ by one-way ANOVA with post hoc Tukey test (**B**-**D**).

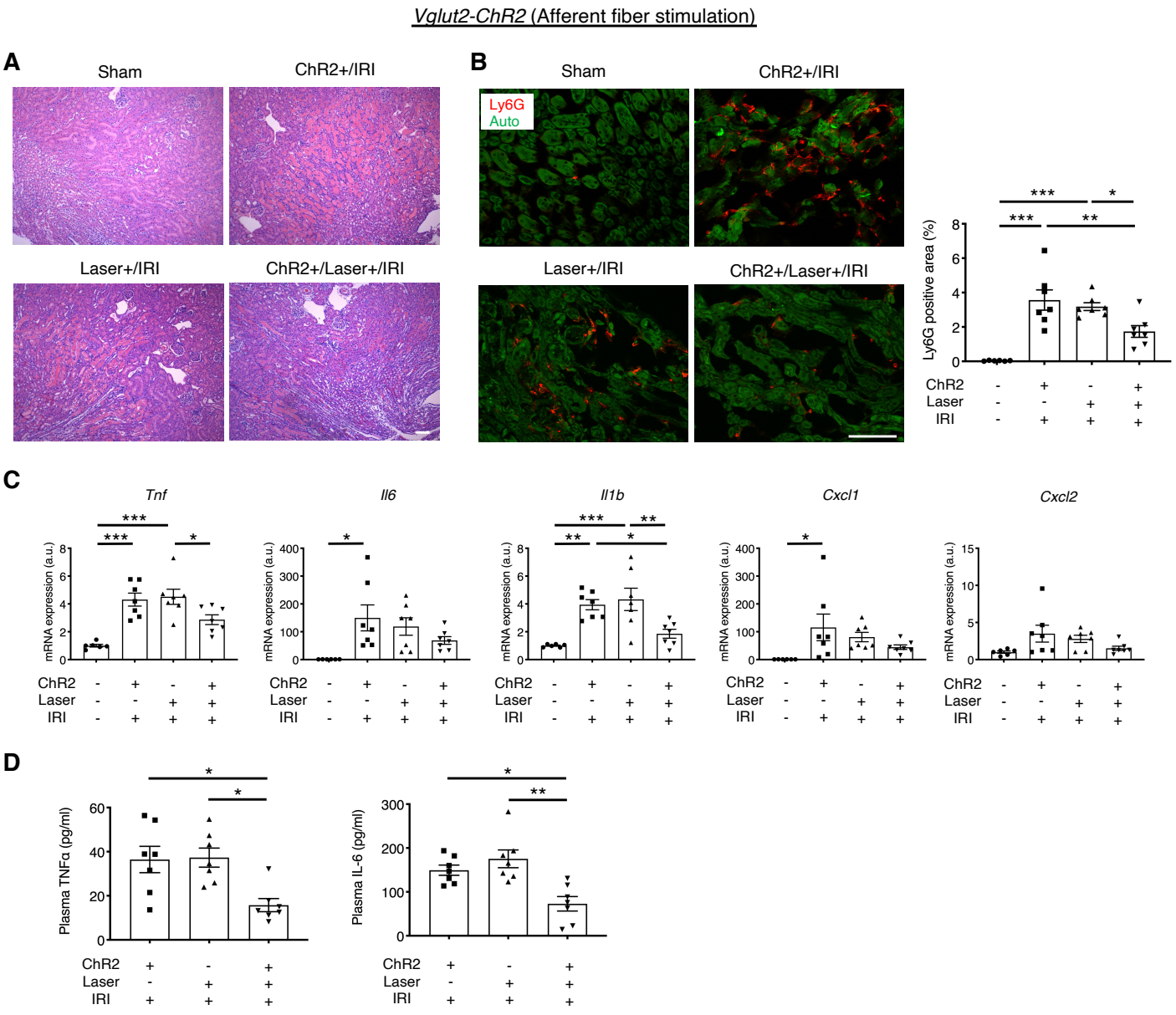

Supplementary Fig. 8. Optogenetic stimulation of vagus afferent fibers protects kidneys against IRI (related to Fig. 2). (**A-D**) Effect of selective afferent fiber stimulation (5 Hz, 10 min) on kidney injury (**A-C**) and plasma cytokine levels (**D**) at 24 h after sham or bilateral kidney IRI in *Vglut2-ChR2* and control mice. (**A**) Photomicrographs taken at lower magnification of H&E staining of representative kidney sections (higher magnification and quantitative analysis of acute tubular necrosis in Fig. 2D). (**B**) Neutrophil staining (Ly6G, red) of kidney with quantification of Ly6G positive area as a percentage of the total surface area of kidney section. Auto: autofluorescence (green). (**C**) Transcript levels of inflammatory cytokines/chemokines (*Tnf*, *Il6*, *Il1b*, *Cxcl1*, *Cxcl2*) in the kidneys. (**D**) Plasma TNFα and IL-6 at 24 h after bilateral kidney IRI were determined

by ELISA. Plasma TNFα and IL-6 were under detection threshold in sham IRI group. n = 6 in sham IRI group and n = 7 in IRI groups (**B**-**D**). Scale bars, 100 μm. Data are represented as mean ± s.e.m. *$P < 0.05$, **$P < 0.01$, and ***$P < 0.001$ by one-way ANOVA with post hoc Tukey test (**B**-**D**).

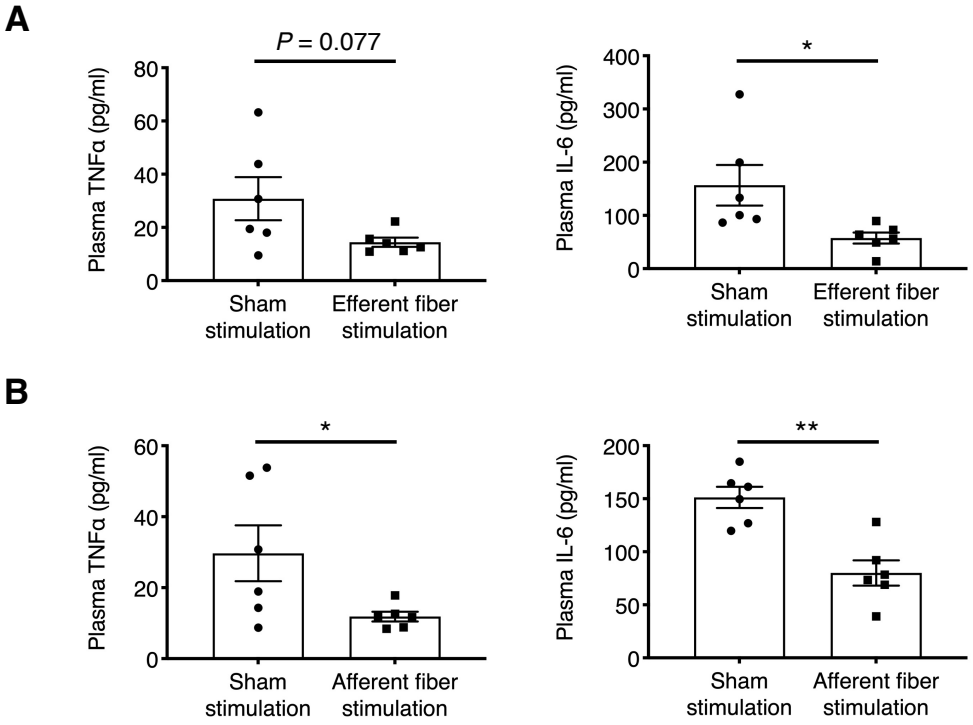

Supplementary Fig. 9. Splenocyte adoptive transfer attenuates circulating inflammatory cytokine levels after IRI. (**A** and **B**) Donor mice underwent optogenetic vagus efferent fiber stimulation (*Chat-ChR2* mice, **A**), afferent fiber stimulation (*Vglut2-ChR2* mice, **B**) or sham stimulation (same trains of laser light delivered to Cre-negative littermates, **A** and **B**), and 24 h later splenocytes were isolated from the donor mice and were injected i.v. (1 x 10^6 cells/recipient mouse) into naïve recipient wild-type mice. The recipient mice were subjected to kidney IRI 24 h after splenocyte transfer. Plasma TNFα and IL-6 at 24 h after bilateral kidney IRI were determined by ELISA. n = 6 in each group. Data are represented as mean ± s.e.m. **P* < 0.05 and ***P* < 0.01 by unpaired two-sided Student's *t* test (**A** and **B**).

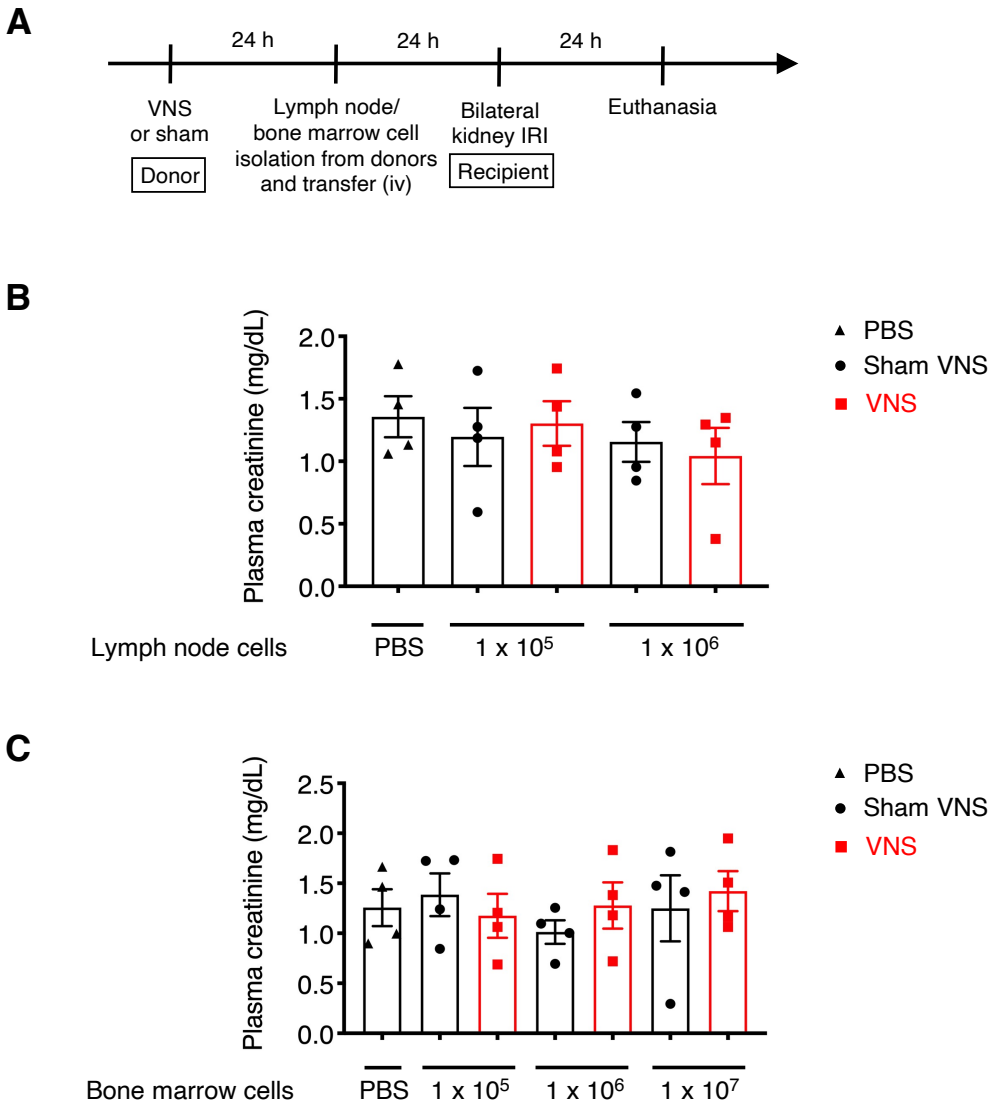

Supplementary Fig. 10. Lymph node cells or bone marrow cells do not play an important role in the protective effect of vagus nerve stimulation against kidney IRI. (**A**) Timeline of experiments for **B** and **C**. (**B**) Plasma creatinine 24 h after bilateral kidney IRI. Donor mice underwent sham VNS or electrical VNS, and 24 h later inguinal lymph node cells were isolated from the donor mice and were injected i.v. (1×10^5 or 1×10^6 cells/recipient mouse) into naïve recipient wild-type mice. PBS was injected i.v. in the control group. The recipient mice were subjected to kidney IRI 24 h after the injection. (**C**) Plasma creatinine 24 h after bilateral kidney IRI. Donor mice underwent sham VNS or electrical VNS, and 24 h later bone marrow cells were isolated from the donor mice and were injected i.v. (1×10^5, 1×10^6 or 1×10^7 cells/recipient mouse) into naïve recipient wild-type mice. PBS was injected i.v. in the control group. The recipient mice were subjected to kidney IRI 24 h after the injection. n = 4 in each group (**B** and **C**). Data are represented as mean ± s.e.m.

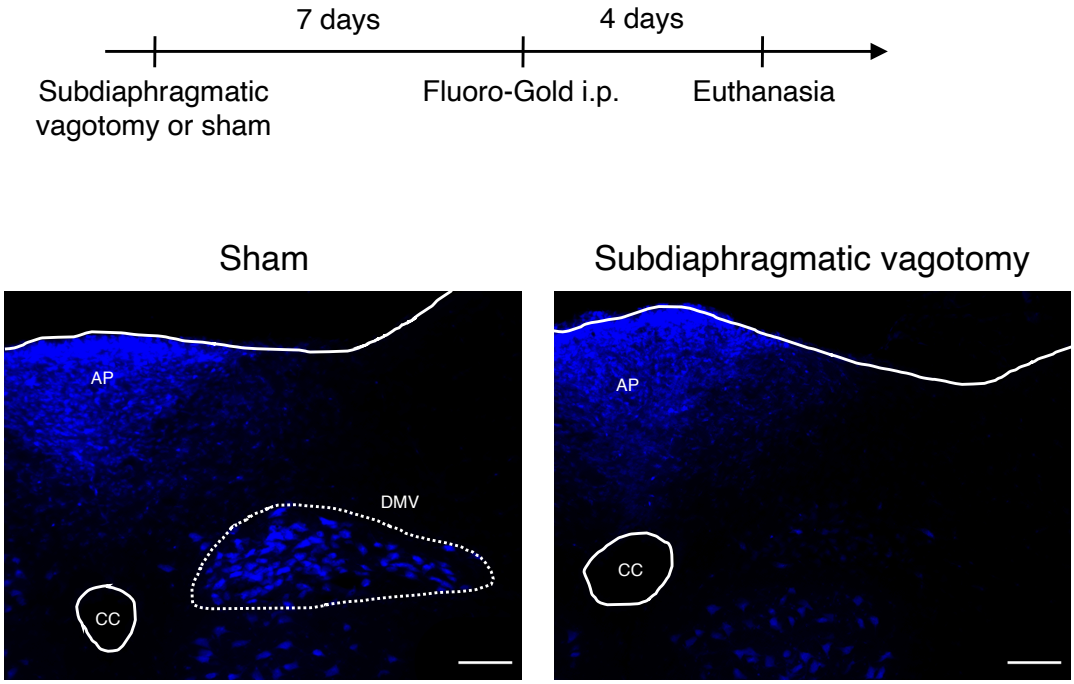

Supplementary Fig. 11. Histological evidence of successful subdiaphragmatic vagotomy. Representative histological picture of the mediodorsal aspect of brainstem sections showing the presence of Fluoro-Gold immunofluorescence (blue) in neurons of the dorsal motor nucleus of the vagus (DMV). Fluoro-Gold is a retrograde tracer – after i.p. injection, it is taken up by nerve terminals in the periphery and transported retrogradely to the brain where cell bodies of origin become labeled. Mice received i.p. injections of Fluoro-Gold seven days after subdiaphragmatic vagotomy or sham surgery. After four days, the mice were euthanized. Note that Fluoro-Gold immunofluorescence in DMV is observed in the sham mouse (because intact vagus nerve terminals can take up Fluoro-Gold) but not in the vagotomized mouse, whereas Fluoro-Gold is present to the same extent in both mice in the area postrema (AP), which lacks the blood–brain barrier. Green autofluorescence was used to reveal the outline of brain sections. CC, central canal. Scale bars: 100 µm.

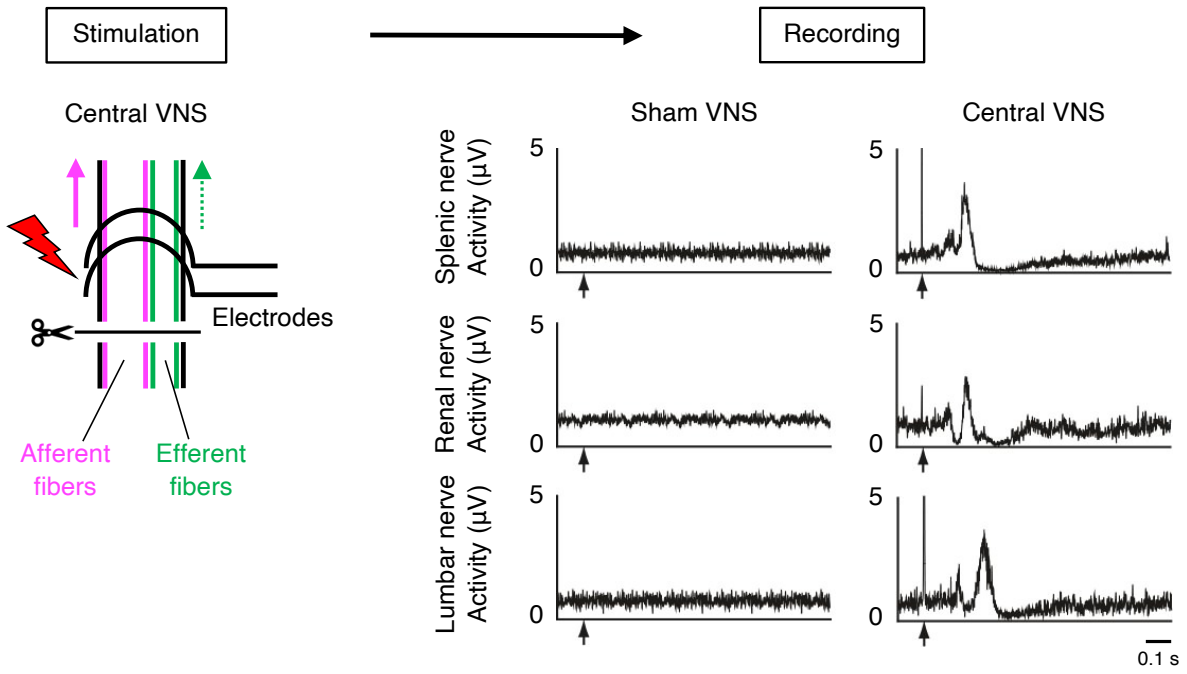

Supplementary Fig. 12. Electrical central VNS activates sympathetic nervous system. Representative recordings of the central VNS-triggered sweeps of amplified evoked potentials at splenic nerve, renal nerve, and lumbar nerve in Sprague-Dawley rats with transection of the left cervical vagus nerve. Central VNS or sham VNS (disconnection between electrodes and the stimulator) were performed for 3 min at 1 Hz (square wave, 150 μA intensity, 1-ms pulses). The averaged evoked potentials were obtained from 180 sweeps in total. Solid and dotted arrows in the illustration indicate action potential transmissions in afferent fibers in an anterograde direction and in efferent fibers in a retrograde direction, respectively. Black arrows indicate stimulation.

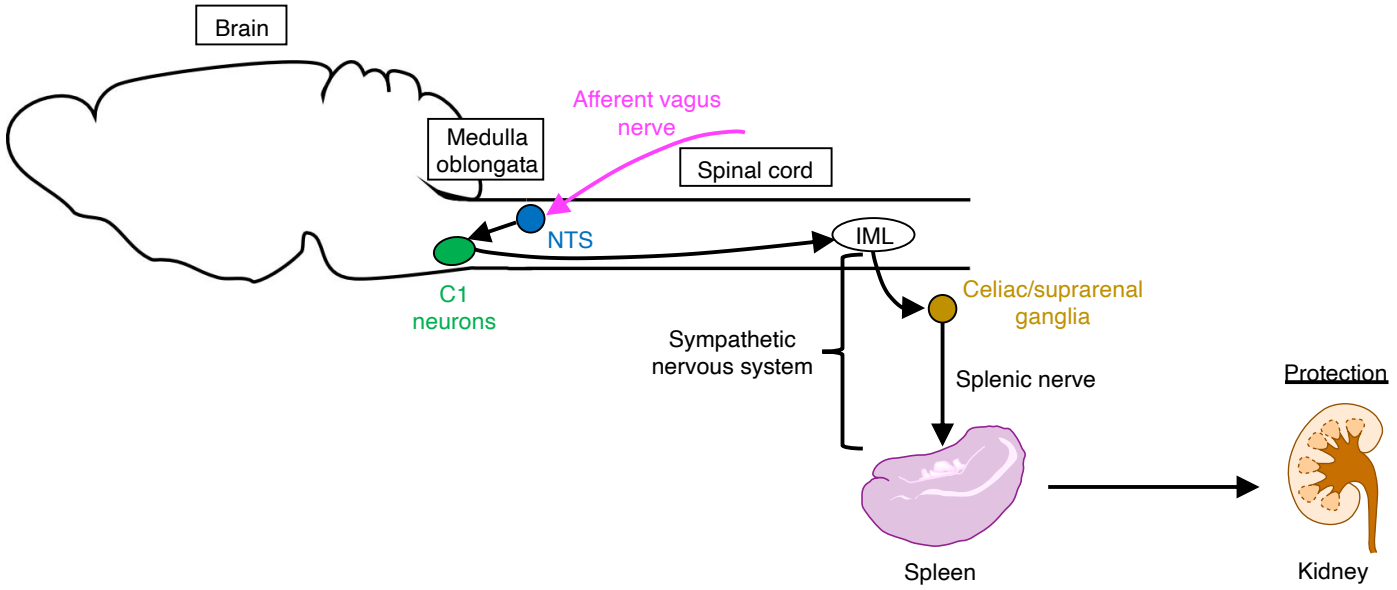

Supplementary Fig. 13. A newly discovered neural circuit involved in the kidney protection by vagus afferent fiber stimulation. Parasagittal view of the brain is shown. Stimulation of afferent vagus nerve activates C1 neurons residing in the medulla oblongata through the nucleus tractus solitarius (NTS), which is an integrative center for sensory information from the vagus nerve. The sympathetic nervous system plays a predominant role as an efferent pathway from C1 neurons, and the signal is transmitted to the spleen through the splenic nerve, which is predominantly a sympathetic nerve. The signal from the splenic nerve probably alters the phenotype of splenocytes as in the canonical CAP activation, which contributes to the kidney protection against IRI. It remains unclear how these splenocytes with an altered phenotype protect the kidney. IML, the intermediolateral cell column.

SI References

1. C. Abe *et al.*, C1 neurons mediate a stress-induced anti-inflammatory reflex in mice. *Nat Neurosci* **20**, 700-707 (2017).
2. T. Inoue *et al.*, Vagus nerve stimulation mediates protection from kidney ischemia-reperfusion injury through alpha7nAChR+ splenocytes. *J Clin Invest* **126**, 1939-1952 (2016).
3. H. M. Perry *et al.*, Dynamin-Related Protein 1 Deficiency Promotes Recovery from AKI. *J Am Soc Nephrol* **29**, 194-206 (2018).
4. J. L. Ardell, W. C. Randall, Selective vagal innervation of sinoatrial and atrioventricular nodes in canine heart. *Am J Physiol* **251**, H764-773 (1986).
5. E. S. Schelegle, J. F. Green, An overview of the anatomy and physiology of slowly adapting pulmonary stretch receptors. *Respir Physiol* **125**, 17-31 (2001).
6. J. O. Foley, F. S. DuBois, Quantitative studies of the vagus nerve in the cat. I. The ratio of sensory to motor fibers. *J Comp Neurol* **67**, 49-67 (1937).